

Magnetic Properties of Ni²⁺(aq) from First Principles

Jiří Mareš,^{*,†} Helmi Liimatainen,[‡] Teemu O. Pennanen,[‡] and Juha Vaara[†]

[†]NMR Research Group, Department of Physics, University of Oulu, P.O. Box 3000, FIN-90014, Oulu, Finland

[‡]Laboratory of Physical Chemistry, Department of Chemistry, University of Helsinki, P.O. Box 55 (A. I. Virtasen aukio 1), FIN-00014, Helsinki, Finland

 Supporting Information

ABSTRACT: The aqueous solution of the Ni²⁺ ion was investigated using a first principles molecular dynamics (FPMD) simulation based on periodic density-functional theory (DFT) calculations. Statistical averages of the magnetic properties corresponding to the triplet spin state of the ion, the hyperfine coupling, g and zero-field splitting tensors, as well as the resulting paramagnetic nuclear magnetic resonance (pNMR) shielding terms were calculated using DFT from instantaneous simulation snapshots extracted from the FPMD trajectory. We report comprehensive tests of the reliability of systematically selected DFT functionals for the properties. The isotropic nuclear shielding of the ¹⁷O nuclei can be obtained with good predictive power. The accuracy of the calculated ¹H shieldings is limited by the fact that the spin-density on the proton sites is not reproduced reliably with the tested functionals, rendering the dominant Fermi contact isotropic shielding term less well-defined. On the other hand, the dominant spin-dipole term of the shielding anisotropy, which gives a practically vanishing isotropic contribution, can be obtained with good reliability for both the ¹H and ¹⁷O nuclei. The anisotropic shielding tensor can be thus utilized reliably in the calculation of Curie-type paramagnetic relaxation. We discuss the evolution of the pNMR properties through the first and second solvation shells of the ion, toward the bulk solvent. The magnetic properties of the dominant, six-coordinated solution are compared to those of the metastable, 5-fold coordinated intermediate occurring in the dissociative exchange process.

INTRODUCTION

A combined molecular dynamics (MD) simulation and molecular properties study provides insight into both static and time-dependent molecular properties not obtainable by static quantum-chemical models. By calculation of the molecular properties along the MD trajectory, both the finite-temperature effect as well as the influence of surrounding molecules (solvent) can be realistically incorporated.^{1–9} Furthermore, properties directly dependent on time such as the magnetic resonance relaxation can be modeled with a greatly decreased number of assumptions.¹⁰ In order to obtain results comparable with experiments, both the MD part as well as the property calculation steps require generally state-of-the-art methods, which usually results in time-consuming studies, thus limiting their number.

As an example of first-principles calculation of nuclear magnetic resonance properties in aqueous systems, Schmidt et al.¹⁰ investigated the quadrupolar NMR relaxation of heavy water using first-principles MD (FPMD) simulations, with the trajectory generated with the forces calculated “on the fly” using density-functional theory (DFT). There have only been a very limited number of studies concerning aqueous solutions of paramagnetic metal ions. Odelius et al.¹¹ calculated the average transient zero-field splitting (ZFS) along an empirical MD trajectory of Ni²⁺ in water, using a preparameterized ZFS hypersurface as a function of distortions from the idealized octahedral geometry. They used the unrestricted Hartree–Fock/restricted configuration interaction method to parametrize the ZFS hypersurface. Recently, Gd³⁺ in water was modeled by FPMD for the calculation of nuclear quadrupole¹² and hyperfine coupling constants (HFCs).¹³ Gd³⁺ in water has also been modeled using empirical

MD and combined with an electron spin resonance (ESR) relaxation study.¹⁴

The hydrated Ni²⁺ ion is a prototypical system for pNMR studies, which has been addressed in a wide range of investigations.^{11,15–20} Detailed understanding of paramagnetic relaxation enhancement (PRE) in such a model system would provide a link toward calculations of magnetic resonance imaging (MRI) contrast agents²¹ as well as applications in structural biology.²² To predict complicated phenomena such as NMR relaxation solely by calculation, it is crucial to be able to validate and recognize the impact of the many approximations that are necessary. In this work, we report an extensive computational study of the ESR and pNMR parameters of the Ni²⁺ ion in aqueous solution, using combined FPMD simulation and quantum-chemical calculations of simulation snapshots. A study of the structure and dynamics of the same system is reported separately.²³ The knowledge of the time evolution of these parameters is necessary for proceeding to dynamic NMR properties, which are experimentally manifested in NMR relaxation.²⁴ Comprehensive results of selected interactions such as transient ZFS and the g tensor for the triplet ($S = 1$) state system, and also a detailed breakdown of the theoretical²⁵ contributions to the average pNMR shielding of water nuclei, is presented both for static six- as well as five-coordinated $\text{Ni}(\text{H}_2\text{O})_n^{2+}$ ($n = 5, 6$) structures and the first and second solvation shells (FSS and SSS) of the dynamical FPMD trajectory. The two coordination cases represent the prevailing situations in the solution as well as the

Received: May 18, 2011

Published: August 04, 2011

Table 1. Basis-Set Dependence of the Orbital and Hyperfine ^1H and ^{17}O Nuclear Magnetic Shielding Constants (in ppm) in $\text{Ni}(\text{H}_2\text{O})_6^{2+}$ Calculated with Density-Functional Theory (PBE Functional)

basis set $\text{H}_2\text{O}/\text{Ni}^a$	number of functions	hydrogen shielding		oxygen shielding	
		orbital part	hyperfine part	orbital part	hyperfine part
aug-pcl0/MK	200	30.4	-215.7	348.7	-17294.7
aug-pcl1/MK	434	29.0	-243.4	357.0	-21139.9
aug-pcl2/MK	848	28.8	-241.4	356.0	-20934.5
aug-pcl0/MK+	248	30.4	-218.7	347.0	-17261.6
aug-pcl1/MK+	482	29.0	-245.0	355.3	-21144.7
aug-pcl2/MK+	896	28.8	-243.6	354.3	-20925.4

^a Notation: O and H basis/nickel basis. MK = Munzarová and Kaupp basis.²⁶ In MK+, partial decontraction is applied, and polarization functions are added (see text).

fleeting intermediate occurring in the dissociative exchange reaction in the FSS,²³ respectively. We were able to witness one such exchange process in our FPMD simulation,²³ which is longer than comparable first-principles studies hitherto performed.

We discuss the accuracy of the models based on a comparison among several available first-principles methods and with experimental data, as well as the general suitability of the FPMD trajectory for the static and dynamic magnetic properties in this system, together with the basis-set convergence. The spin density distribution and magnetic properties, HFC, g, and ZFS tensors, as well as the pNMR shieldings, are reported.

RESULTS AND DISCUSSION

Detailed descriptions are included in the Supporting Information about the methods used for static models of the first solvation shell, FPMD simulations, as well as property calculations on simulation snapshots.

Basis Set Selection for the $\text{Ni}(\text{H}_2\text{O})_6^{2+}$ Complex. The results for the basis-set convergence for the calculation of NMR/ESR properties are listed in Table 1. The largest changes between results obtained with different hydrogen and oxygen basis sets are seen between aug-pcl0 and aug-pcl1, whereas aug-pcl2 only brings a small further modification. Improving the MK basis for Ni by diffuse/polarization functions and partial decontraction (MK+) similarly produces only a slight change of results. Therefore, for production calculations, the aug-pcl1/MK combination of basis sets was selected.

Methods for pNMR Shielding along the MD Trajectory. To assess the extent of the region that is significantly influenced by the paramagnetic center (Figure 1), we first tested the radial decay properties of the spin density at the PBE/SVP level. The spin density decays very rapidly around the metal ion, so that relatively little is left, on average, in SSS. On the basis of these data, we decided to include the complete FSS and SSS in our production calculations using the larger basis sets. Although SSS is relatively well-defined on average, in instantaneous configurations, its border to bulk water is not clear. We considered every water molecule that has at least one atom closer than 5 Å from the central ion, to belong to SSS. In this context, we noticed that the implicit solvation model (COSMO for the ESR tensors calculated with ORCA,²⁷ as well as PCM for the orbital shielding in G03²⁸) both improves the self-consistent field (SCF) convergence and prevents the occasional occurrence of spurious high spin density in the outer regions of the calculated snapshots

clusters. These implicit solvation models were therefore used in all further snapshot calculations. The explicit solvation of the selected SSS region was accomplished by including in the snapshot calculations all the water molecules that have at least one atom closer than 7 Å from the central atom. This layer corresponds roughly to the extent of the third solvation shell of the Ni^{2+} ion. This procedure resulted in clusters that contained on average 55.36 water molecules, of which 16.07 were in SSS, with FSS consisting most of the time of the six nearest neighbors of the ion. These numbers fluctuated in the ranges 48–63 and 10–22 for the total size of the cluster and SSS, respectively. To significantly decrease the computational cost, the small SVP basis was used beyond SSS. Our tests proved that a completely negligible effect resulted from using the SVP basis as compared to a calculation, in which the larger basis set was used throughout. A total of 2469 such clusters were sampled from the equilibrated part of the trajectory of the system containing 127 water molecules.

Structure of the Solvated Ni^{2+} Ion. The structural parameters for various combinations of methods are reported in a related work.²³ Briefly, in the six-fold structure, the oxygen atoms are octahedrally coordinated, whereas the symmetry of the whole complex is weakened by the increasing tilt angle of the water molecules, defined as the angle between the Ni–O vector and the HOH bisector. The 5-fold coordinated complex forms a tetragonal pyramid. The same is true for the coordination found in the corresponding parts of the FPMD simulation trajectory. As an example, frequently used in further calculations, the static calculations using PBE *in vacuo* and PBE together with the COSMO solvation model can be taken. The first results in a Ni–O distance of 2.086 Å and tilt angle of 23.0°, whereas the COSMO structure was 2.076 Å and 45.7°, the latter resembling the average FPMD structure.

Hyperfine Couplings in the $\text{Ni}(\text{H}_2\text{O})_6^{2+}$ and $\text{Ni}(\text{H}_2\text{O})_5^{2+}$ Complexes. To compare the impact of various exchange-correlation functionals (ECFs) on the isolated and hexa- and penta-coordinated dications, we selected a single structure obtained by geometry optimization at the PBE/def2-TZVP level. The Fermi contact term A_{con} , the largest (in absolute value) principal value of spin-dipole tensor A_{dip} (denoted as A_{33}^{dip}), as well as the rhombicity ($\text{Rh}(X) = X_{22} - X_{11}$) $\text{Rh}(A_{\text{dip}})$ of the HFC tensor were calculated for both the ^1H and ^{17}O nuclei. One set of calculations was carried out *in vacuo*, i.e., no explicit or implicit solvation model was applied around $\text{Ni}(\text{H}_2\text{O})_6^{2+}$. The results are illustrated in Figures 2 and 3 for ^1H and ^{17}O , respectively. Both the A_{con} and A_{33}^{dip} parameters develop systematically with the exact exchange admixture in the

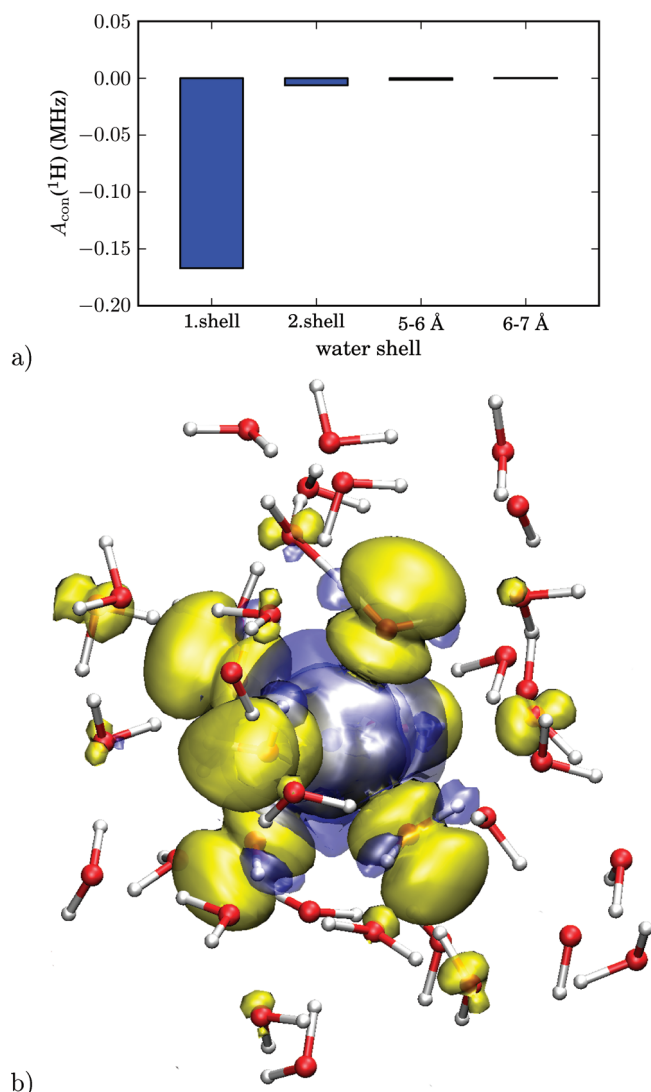


Figure 1. (a) Simulated Fermi contact hyperfine coupling constant at the ^1H nuclei in an aqueous solution of Ni^{2+} ion, as a function of increasing distance from the metal center. The presented values are averages over 10 randomly chosen snapshots calculated using the PBE/SVP level of theory, together with the COSMO solvation model. (b) Spin density in a random simulation snapshot. The yellow isosurface shows the positive spin density of 0.0001 au, whereas the blue isosurface indicates a negative spin density of the same absolute value. The spin density is taken from the periodic QUICKSTEP²⁹ calculation in which the PBE/DZVP level of theory was used.

ECF. Large relative differences are observed among the $A_{\text{con}}(^1\text{H})$. To produce these data, all structures were obtained with the def2-TZVP basis set, and for the property calculations, the aug-ccpV1/MK combination was used for O, H/Ni. Tabulated numerical data can be found in Tables S2 and S3 in the Supporting Information. The $A_{33}^{\text{dip}}(^1\text{H})$ exhibits a weaker, although equally systematic dependence on the choice of the ECF and is roughly one magnitude larger in absolute value. The situation is different for the ^{17}O nuclei, where A_{con} dominates over the spin-dipole part. The largest absolute value of A_{con} (-35.83 MHz for BLYP) is almost twice as large as the smallest among the tested set of methods (-20.40 MHz using SCS-MP2).

To test the direct impact of the solvation model on the calculated hyperfine properties, we used the same PBE/def2-TZVP/*in vacuo*

structure but employed the COSMO solvation model for the hyperfine calculation. In the scale of the differences among different methods (ECFs or SCS-MP2), the impact of the implicit solvation model in the property calculation step is entirely negligible. To test, on the other hand, the indirect impact of the COSMO solvation model on properties via its effect on the structure, we performed the property calculation also using PBE/def2-TZVP/COSMO structures. The latter differ significantly from the corresponding *in vacuo* structures, both in the Ni–O distance and tilt angle. The largest relative change is observed for $A_{\text{con}}(^1\text{H})$, proportional to the spin density on these nuclei, where not only the absolute value but even the sign changes. The influence of using the COSMO structure on the spin dipole contribution to ^1H and both $A_{\text{con}}(^{17}\text{O})$ and $A_{33}^{\text{dip}}(^{17}\text{O})$ is relatively less important but still numerically significant. The absolute values of the dipolar contributions for both ^1H and ^{17}O increase due to using the implicitly solvated structure, whereas $A_{\text{con}}(^{17}\text{O})$ decreases.

We have further consistently optimized all structures with the same functional (or SCS-MP2) as the one used for the property calculation and obtained data sets, both using COSMO and *in vacuo*. Subsequently, the properties were calculated only using, for simplicity, the COSMO model (the influence of COSMO in the property step is seen above to be minor). For the COSMO structures, $A_{\text{con}}(^1\text{H})$ and $A_{\text{con}}(^{17}\text{O})$ span a narrower range as compared to the two data sets obtained using the PBE structures. This implies that using structure optimization at the same level as used for the property calculation may be the preferred choice for hyperfine properties.³⁰

We have done all of the above calculations also for the 5-fold coordinated Ni^{2+} ion. The results are plotted to the same scale as for the 6-fold coordinated case, in Figures 2 and 3. Upon the change from 6- to 5-fold coordination, there is a clear increase of the magnitude of the dipolar contribution for the ^1H nuclei and a slight increase for the ^{17}O nuclei (in absolute value) in all of the calculated static structures, as well as in the average values over the FPMD trajectory. This observation is in accordance with the shortened distances between Ni^{2+} and the nuclei in question. For the contact term, only a very slight and nonuniform change takes place for the ^1H nuclei. For ^{17}O , we observe a slight decrease in the magnitude of A_{con} in 32 of the 36 tested static calculations, as well as in the FPMD average.

The overall conclusion is that the signs and orders of magnitude are well-defined across the different levels of theory used, for the presently relevant HFC parameters other than $A_{\text{con}}(^1\text{H})$. In light of these results, the agreement between the results from the experiment³¹ [$A_{\text{con}}(^1\text{H}) = -0.13$ MHz] and PBE (COSMO/COSMO for properties/structure; -0.15 MHz; Table S2) should be considered rather fortuitous. The results show that it is important to account for solvation effects on the underlying molecular structures.

g Tensor. The g tensor parametrizes the Zeeman interaction of the electronic spin with the magnetic field and enters the hyperfine terms of the pNMR shielding. In particular, the s.c. g shift tensor, $\Delta g = g - g_e \mathbf{I}$, i.e., the deviation from the isotropic free-electron g factor ($g_e \approx 2.0023$), is a nontrivial quantity to compute. In complete analogy to the test discussed above concerning HFC, we tested the performance of the available ECFs, the inclusion of a solvation model, as well as the dependence on the structure obtained by different methods. The results are graphically presented in Figure 4 and tabulated in Table S4, Supporting Information. We observe that also the g value is systematically dependent on the exact exchange admixture of the ECF, with the g value rising with an increasing fraction of the exact exchange. We lack presently efficient tools for

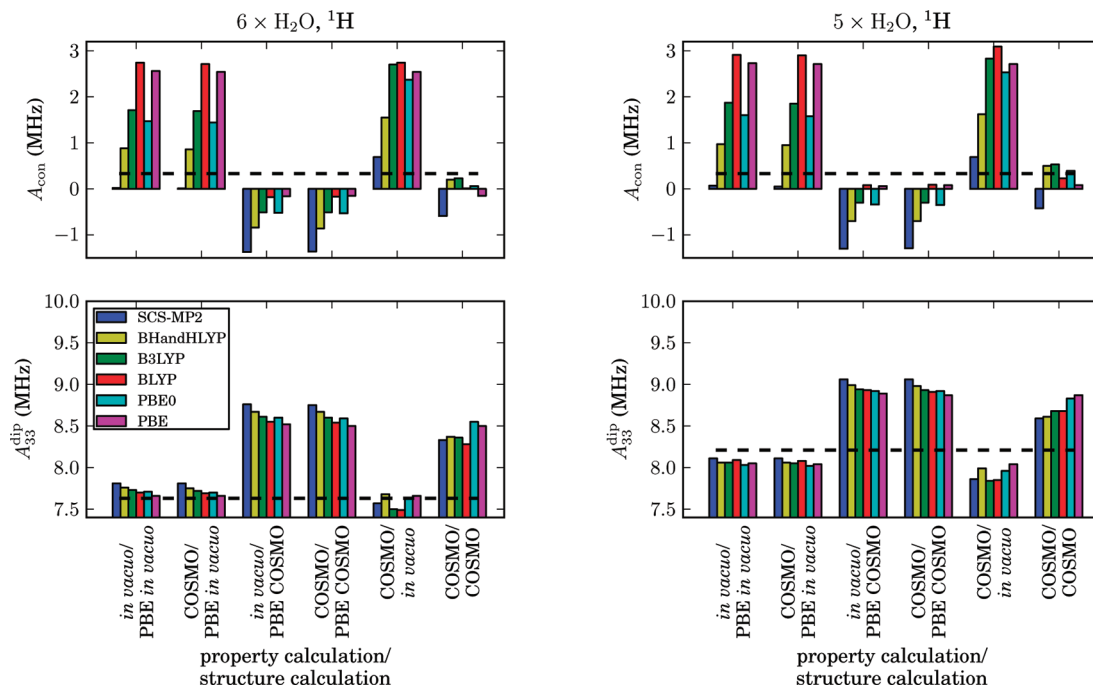


Figure 2. Impact of the choice of the DFT exchange-correlation functional on the average Fermi contact (con) and spin-dipole (dip) part of the ${}^1\text{H}$ hyperfine coupling (MHz) in $\text{Ni}(\text{H}_2\text{O})_6^{2+}$. The results of the SCS-MP2 calculations are presented for comparison. For the first four sets, the structures were obtained using the PBE functional, whereas for the last two sets, the structures were obtained with the same functional as the properties. All values present averages over all nuclei. Only the largest eigenvalue (in absolute value) A_{33} of the spin-dipole tensor is plotted. The dashed lines illustrate the average values obtained from the FPMD simulation (using PBE both for the trajectory and for the properties) of 127 water molecules and one Ni^{2+} ion. The corresponding (6- or 5-fold coordinated Ni^{2+} ion) parts of the trajectory were used for obtaining these values.

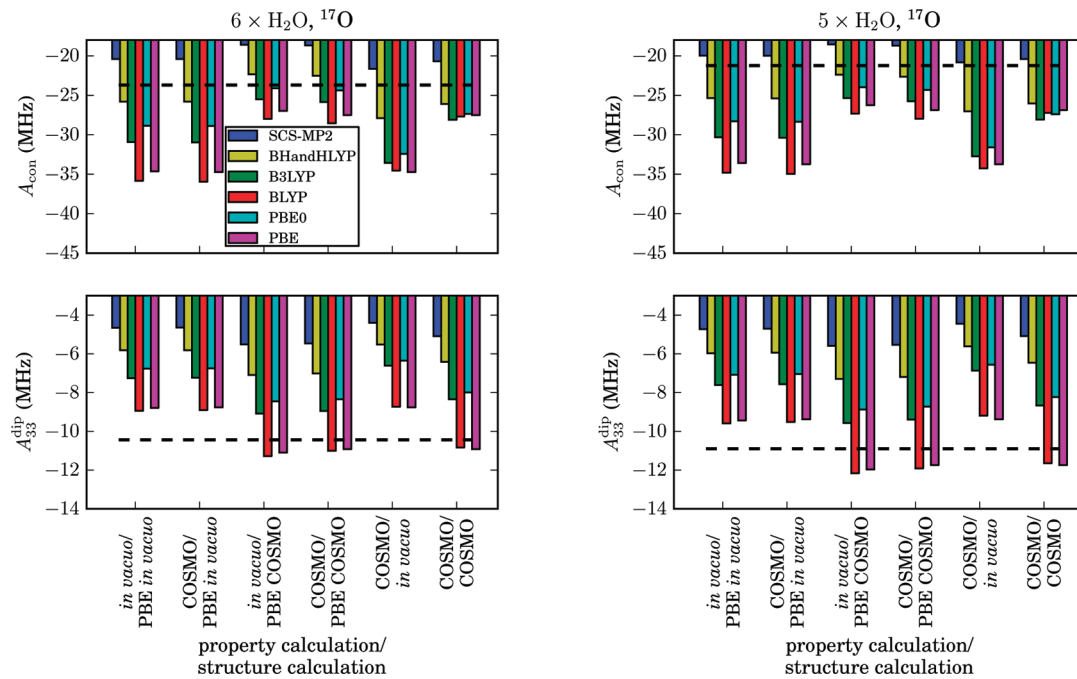


Figure 3. As for Figure 2, but for ${}^{17}\text{O}$.

obtaining *ab initio* estimates for the g value in these complexes, although an implementation at the coupled-cluster singles and doubles (CCSD) level of theory has already been reported.³² Such tools would be highly useful for calibrating the DFT

performance, as no direct experimental results on the g tensor have been reported for the present system.

With any present ECF, the obtained g value is larger by 0.01–0.02 for the 5-fold than for the 6-fold coordinated ion.

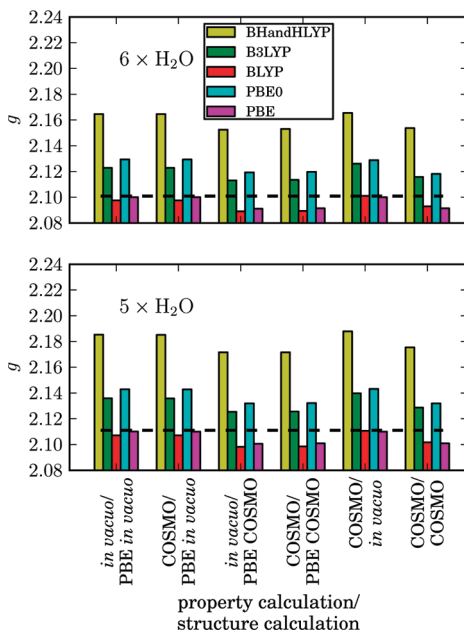


Figure 4. As for Figure 2, but for the isotropic g values.

Second, the g value is always smaller by roughly the same amount for the 5- and 6-fold coordinated structures obtained with the solvation model than for the corresponding *in vacuo* structures. The structures obtained with COSMO generally have a larger tilt angle and shorter Ni–O distance than structures obtained without the solvation model.²³ Similarly to the HFC tensor, the effect of using the implicit solvation model in the property calculation step is found to be negligible for the g tensor. In contrast to HFC, however, using the same ECF both for the structure and for the g tensor does not change the results appreciably, as compared to using PBE for structures.

Averages obtained from the MD snapshots using the PBE functional indicate that the combined dynamic and solvation influence on the g value is only 0.001 for both the six- and five-coordinated situations (compared to *in vacuo* static structures), indicating partial cancellation of the two effects. A notable feature apparent in the plot of the g value along the MD trajectory (Figure 5) is its increase in the last part of the trajectory, when the system enters the intermediate, 5-fold coordinated situation. In this part of the trajectory, the parallel component g_{\parallel} can be defined by the direction of the “missing” water molecule. This component remains close to the isotropic value of the 6-fold coordinated average, whereas the perpendicular component g_{\perp} is responsible for the increase of the isotropic value.

The simulated g values are higher by up to 0.01 than the results of all static FSS models, when the data obtained by the same (PBE) functional are compared. Furthermore, the simulation verifies the size of the increase of g from the 6-fold-coordinated to the 5-fold-coordinated model, obtained using the static $\text{Ni}(\text{H}_2\text{O})_n^{2+}$ ($n = 5, 6$) structures.

Experimental data are available for the crystals of nickel Tutton salts, which contain Ni^{2+} coordinated by six water molecules.³³ The average g value for these compound is 2.25. The same value was later adopted also in an EPR relaxation study of the aqueous solution of Ni^{2+} .³⁴ The values of 2.25 and 2.3 have been also used in NMR studies of aqueous Ni^{2+} solutions (refs 35 and 31, respectively). Our static DFT calculations using different ECFs

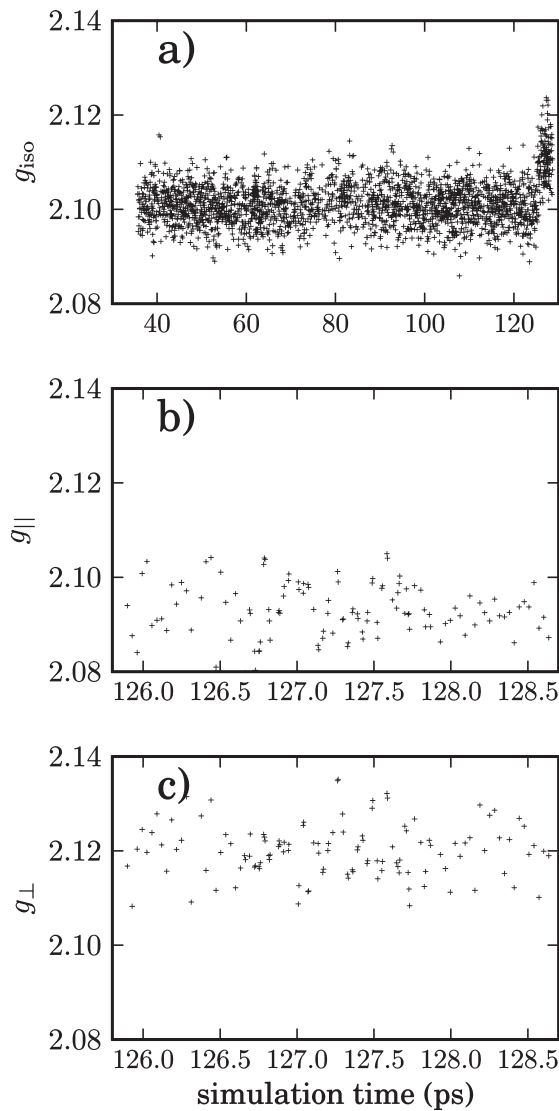


Figure 5. Calculated g tensor plotted along a first-principles molecular dynamics trajectory of the Ni^{2+} ion in the aqueous solution. The increase at the end of the trajectory (a) corresponds to a situation with a 5-fold coordinated Ni^{2+} ion. In panels b and c, parallel and average perpendicular eigenvalues are plotted for the 5-fold coordinated part of the trajectory. Here, g_{\parallel} and g_{\perp} are defined as the components of the g tensor along with and perpendicular to, respectively, the direction from the Ni^{2+} ion to the “missing” water molecule in the originally octahedral complex. The PBE functional was used for the system with 127 water molecules.

as well as the dynamic simulation point to significantly smaller g values. This implies that the assumption that the g value is the same in both salt crystal and liquid solution is questionable.

Zero-Field Splitting. The effect of the ZFS Hamiltonian

$$H_{\text{ZFS}} = \mathbf{S} \cdot \mathbf{D} \cdot \mathbf{S} \quad (1)$$

on the energy levels within the spin manifold of an $S \geq 1$ species is best characterized with parameters

$$D = D_{33} - \frac{1}{2}(D_{11} + D_{22}) \quad (2)$$

$$E = \frac{1}{2}(D_{22} - D_{11}) \quad (3)$$

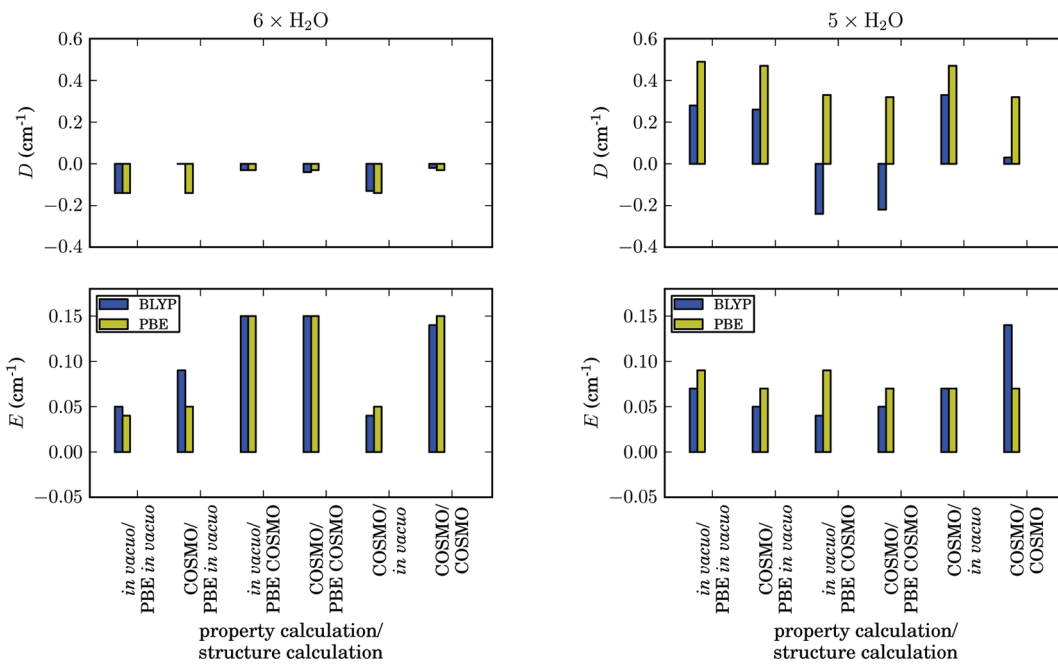


Figure 6. As for Figure 2, but the D and E parameters of the zero-field splitting tensors are presented. In all calculations, the same selection of the principal axis system defining the D and E parameters [eqs 2–3] was used so that similar geometries have similar orientations of the ZFS axis system.

expressed in terms of the eigenvalues D_{ii} of the \mathbf{D} tensor. The ordering of the principal values is selected so that $0 \leq E/D \leq 1/3$.^{36,37}

In the calculation of the ZFS tensor, we tested two GGA functionals, PBE and BLYP, the inclusion/omission of the solvation model as well as the dependence on the structure obtained by different methods. The same calculations were carried out for both $\text{Ni}(\text{H}_2\text{O})_n^{2+}$ ($n = 5, 6$) complexes. The results are plotted in Figure 6, and the numerical data are contained in Table S5, Supporting Information. In the upper right panel of Figure 6, the discrepancy between BLYP and PBE functionals when COSMO structures are used is caused by the poor alignment between the principal axis of the ZFS tensor and the molecular axis system. The negative sign in the two cases of the D parameter determined by BLYP is therefore not entirely relevant. Since the structure of the 6-fold coordinated Ni^{2+} ion is highly symmetric, the resulting D and E values are expectedly close to zero. The symmetry is broken in the 5-fold coordinated ion.

For the calculations of snapshots extracted from the FPMD dynamics, it is important to consider the choice of the axis system. For any instantaneous configuration, a proper axis system can be found such that the D and E parameters can be calculated in the same way as described above. The time evolution of these parameters at the PBE level is plotted in Figure S1, Supporting Information. Clearly, both D and E vanish on average for an isotropic solution of the symmetrically coordinated ion. In this case, there is no choice of the axis system that would be unique and constant over time. For the 5-fold coordinated part of the trajectory, similarly as for the \mathbf{g} tensor, the parallel component $D_{||}$ can be defined by the direction from the nickel ion to the “missing” water molecule. The D and E parameters of the ZFS tensor are then given by eqs 2 and 3 with $D_{33} = D_{||}$, D_{11} and D_{22} being the perpendicular components. The RMS values of D , E , and E/D can be found for

the 5-fold-coordinated part of the trajectory in Table 2. For the 6-fold-coordinated part, which is on average octahedrally symmetric, the RMS value of the scalar tensor product (Δ)

$$\Delta = \sqrt{\langle \mathbf{D}(0) : \mathbf{D}(0) \rangle} = \sqrt{\langle \sum_{\alpha\beta} D_{\alpha\beta}(0) D_{\alpha\beta}(0) \rangle} \quad (4)$$

serves as a parameter characterizing the fluctuations of the ZFS tensor. For comparison, we also performed an analysis equivalent to that of Odelius et al.¹¹ and calculated the time-correlation function (TCF) of the scalar tensor product $\langle \mathbf{D}(0) : \mathbf{D}(\tau) \rangle$ (TCF_{ZFS}). The normalized autocorrelation function is plotted in Figure 7. The value of the normalized TCF decays to less than 0.1 in a little over 100 fs and slowly decreases to the noise level during the following ca. 4 ps.

In our simulation, the decay of the TCF does not exhibit the well-defined damped oscillatory character seen by Odelius et al. with a period of roughly 90 fs. In their work, they obtain the instantaneous ZFS tensor from a preparameterized function involving the geometrical distortions of the octahedral complex along two classes of modes corresponding to $\text{Ni}-\text{O}$ bond vibrations (E_g modes) and oscillation of the $\text{O}-\text{Ni}-\text{O}$ angle. The dependence on other modes, namely, the rotational mode of the water molecules, was omitted. The oscillatory TCF of the E_g modes is almost identical to TCF_{ZFS} . It may be speculated that the remaining geometrical dependences cause the TCF_{ZFS} to be more damped. According to our calculation, the ZFS tensor is more sensitive to molecular geometry than what the model of Odelius et al. assumed. For example, the $\langle \mathbf{D}(0) : \mathbf{D}(\tau) \rangle$ curve from our work is damped to an extent that no anticorrelation can be observed. Also, the calculated RMS value Δ yields 100 cm^{-1} in our study for the 6-fold coordinated part of the FPMD trajectory, which is an order of magnitude higher than that of Odelius et al. ($\sim 5.2 \text{ cm}^{-1}$).¹¹ The reason for such a large difference is presently unclear to us.

Table 2. Calculated EPR and NMR Parameters of the Aqueous Solution of Ni²⁺^a

	6 × H ₂ O ^b	5 × H ₂ O ^c
g_{iso}^d	2.1009 ± 0.0002	2.1110 ± 0.0004
g_{iso} (exptl) ^e	2.25	
RMS(D) (cm ⁻¹) ^f		14.6
RMS(E) (cm ⁻¹) ^g		5.1
RMS(E/D)		9.1
Δ (cm ⁻¹) ^h	100	13.9
Δ_5 (cm ⁻¹) ⁱ	45	6.2
Δ_5 (cm ⁻¹ ; exptl) ^j	2.6	
$A_{\text{con}}(^1\text{H})$	0.33 ± 0.07	0.33 ± 0.07
$A_{\text{con}}(^{17}\text{O})$	-23.7 ± 0.3	-21.2 ± 0.4
$A_{\text{dip},33}(^1\text{H})^k$	7.63 ± 0.02	8.21 ± 0.03
$A_{\text{dip},33}(^{17}\text{O})^k$	-10.44 ± 0.05	-10.9 ± 0.2
$\text{Rh}[\text{A}_{\text{dip}}(^1\text{H})]^l$	2.73 ± 0.02	3.06 ± 0.02
$\text{Rh}[\text{A}_{\text{dip}}(^{17}\text{O})]^l$	0.090 ± 0.002	0.38 ± 0.09
$A_{\text{iso}}(^1\text{H})^m$	0.30 ± 0.07	0.29 ± 0.07
$A_{\text{iso}}(^{17}\text{O})^m$	-23.5 ± 0.3	-20.9 ± 0.4
$A_{\text{iso}}(^1\text{H})$ (exptl)	0.13 ± 0.01 ⁿ	
$A_{\text{iso}}(^{17}\text{O})$ (exptl)	24. ^o - 28.2 ^p	
$\sigma_{350\text{K}}^{\text{iso}}(^1\text{H})$	6 ± 4	
$\sigma_{350\text{K}}^{\text{iso}}(^{17}\text{O})$	-10960 ± 90	
$\sigma_{350\text{K}}^{\text{iso}}(^1\text{H})$ (exptl)	34 ^q	
$\sigma_{350\text{K}}^{\text{iso}}(^{17}\text{O})$ (exptl)	-10988, ^r -9938 ^s	

^a First principles molecular dynamics using the PBE functional and 127 water molecules. Experimental results are listed where available. ^b The six-coordinated part of the simulation trajectory, statistics over 2000 snapshots.

^c The five-coordinated part of the simulation trajectory, statistics over 120 snapshots. ^d The corresponding g shift value would be obtained by subtracting the free-electron value $g_e = 2.0023$. ^e Ref 33. Measurement on hydrated Ni²⁺ salt crystals. This value has, however, been used also for Ni²⁺ solutions in the literature. ^f For the five-coordinated complex, the parallel axis is in the direction of the “missing” water molecule in the originally octahedral complex; then, $D = D_{\parallel} - 1/2(D_{\perp,1} + D_{\perp,2})$. For the 6-fold coordinated complex, these quantities are not clearly defined (see text). ^g As

footnote ^f, but $E = 1/2(D_{\perp,1} - D_{\perp,2})$. ^h RMS obtained from the average scalar tensor product eq 4. ⁱ $\Delta_5 = \langle (\mathbf{D}(0) \cdot \mathbf{D}(0)) / 5 \rangle^{1/2}$ (here, the factor 5 is the number of independent components needed to specify the ZFS tensor). The numbers are added for consistency with the literature experimental value (footnote ^j). ^j Ref 34. Electron spin relaxation study based on proton NMR relaxation measurement in aqueous Ni²⁺ solution. ^k The largest (in absolute value) value of the eigenvalues of the traceless tensor. ^l Rhombicity of the dipolar tensor, $\text{Rh}(\text{A}_{\text{dip}}) = A_{22}^{\text{dip}} - A_{11}^{\text{dip}}$. The values are very small for the oxygen nuclei in the 6-fold-coordinated complex, in agreement with the nearly octahedral symmetry. ^m The isotropic value contains both the Fermi contact and spin-orbit contributions, the latter being much smaller. ⁿ Ref 31. The hyperfine coupling constant was reported without sign, an inspection of the data points to the negative sign. ^o Ref 35. The hyperfine coupling constant was reported without sign. ^p Ref 38. ^q This value of the shielding constant was obtained by extrapolation of the experimental data measured in the range of 243.15–263.15 K³¹ assuming a 1/T dependence of the paramagnetic chemical shifts. Furthermore, pure water in gas phase (PBE) was taken as the reference, $\sigma_{\text{ref,gas}}(^1\text{H}) = 31.59$ ppm with a gas-to-liquid shift correction (B3LYP) $\delta_{\text{gas} \rightarrow \text{liquid}}(^1\text{H}) = -5.27$ ppm,⁶ see the main text.

^r The value of the shielding constant was obtained by extrapolation of the experimental data measured in the range of 274.65–306.15 K³⁵ assuming a 1/T dependence of the paramagnetic chemical shifts. Referenced and corrected for gas-to-liquid shift as in footnote ^q using the values for ¹⁷O: $\sigma_{\text{ref,gas}}(^{17}\text{O}) = 324.8$ ppm, $\delta_{\text{gas} \rightarrow \text{liquid}}(^{17}\text{O}) = -41.2$ ppm. ^s From the experimental data measured in the range of 243.65–308.15 K.³⁸ Referenced and corrected for the gas-to-liquid shift as in footnote ^r.

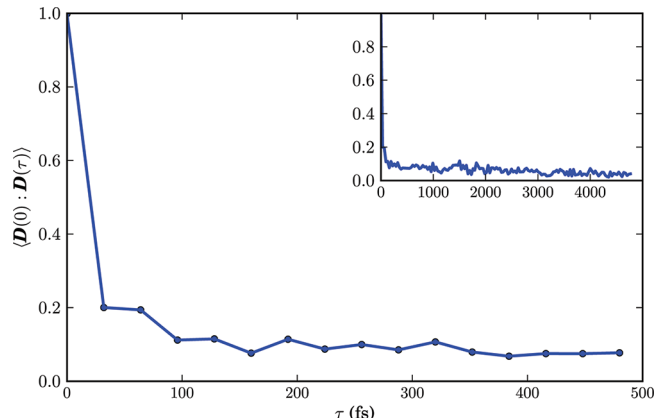


Figure 7. Simulated time correlation function $\langle \mathbf{D}(0) : \mathbf{D}(\tau) \rangle$ of the scalar tensor product of the zero-field splitting tensor of the aqueous solution of Ni²⁺. First-principles molecular dynamics using the PBE functional and 127 water molecules.

Nuclear Shielding in the Static Structures. We present calculated shielding contributions using the static 5- and 6-fold-coordinated Ni(H₂O)_n²⁺ optimized both *in vacuo* and with the COSMO implicit solvation model. We use the classification and nomenclature of the terms set forth in the general shielding theory for species of arbitrary spin multiplicity, in ref 25. In particular, and as described in the Supporting Information, the theory predicts for a higher-than-doublet system several new isotropic shielding contributions as compared to the case of the doublet.³⁹ In the present triplet system, however, the influence of these new terms turns out to be small.

In the calculation of the nuclear shielding contributions, in analogy to the tests of the HFC, g and ZFS tensors, we have tested the performance of the present set of ECFs, inclusion/omission of the solvation model, and the dependence on the structure obtained by different methods. The results are summarized in Figures 8 and 9, and the numerical data are given in Tables S6–S9, Supporting Information.

The observations at different levels of theory are parallel to the corresponding experience with HFC. The total isotropic shielding is dominated by the contact term for both the ¹H and ¹⁷O nuclei. For ¹H, there is a major influence of the structure at which the shielding tensor is calculated. For the structures obtained *in vacuo*, the ¹H contact shieldings have a sign opposite that for the structures obtained with the implicit COSMO solvent model. In the case of ¹⁷O, the use of COSMO structures leads to a reduction of the contact term by 1000–3000 ppm.

For all of the terms, there is a clear dependence of the observed value on the amount of the exact exchange admixture. This is particularly important for the dominating contact term. In contrast, all of the hyperfine shielding terms exhibit only a minor dependence on the use of the COSMO model at the property calculation step. The solvent effect arises mainly indirectly, via the structure. The orbital shielding σ_{orb} changes, however, also upon the introduction of the PCM solvent model in the property calculation step.

Apart from the nonrelativistic σ_{con} and σ_{orb} contributions, the isotropic shielding obtains contributions from $\sigma_{\text{con},2}$ and $\sigma_{\text{con},3}$ terms arising from the relativistic spin-orbit contributions to the HFC and g tensors, respectively. None of the other terms contribute numerically significantly. In particular, both the pseudocontact and the novel isotropic terms introduced in

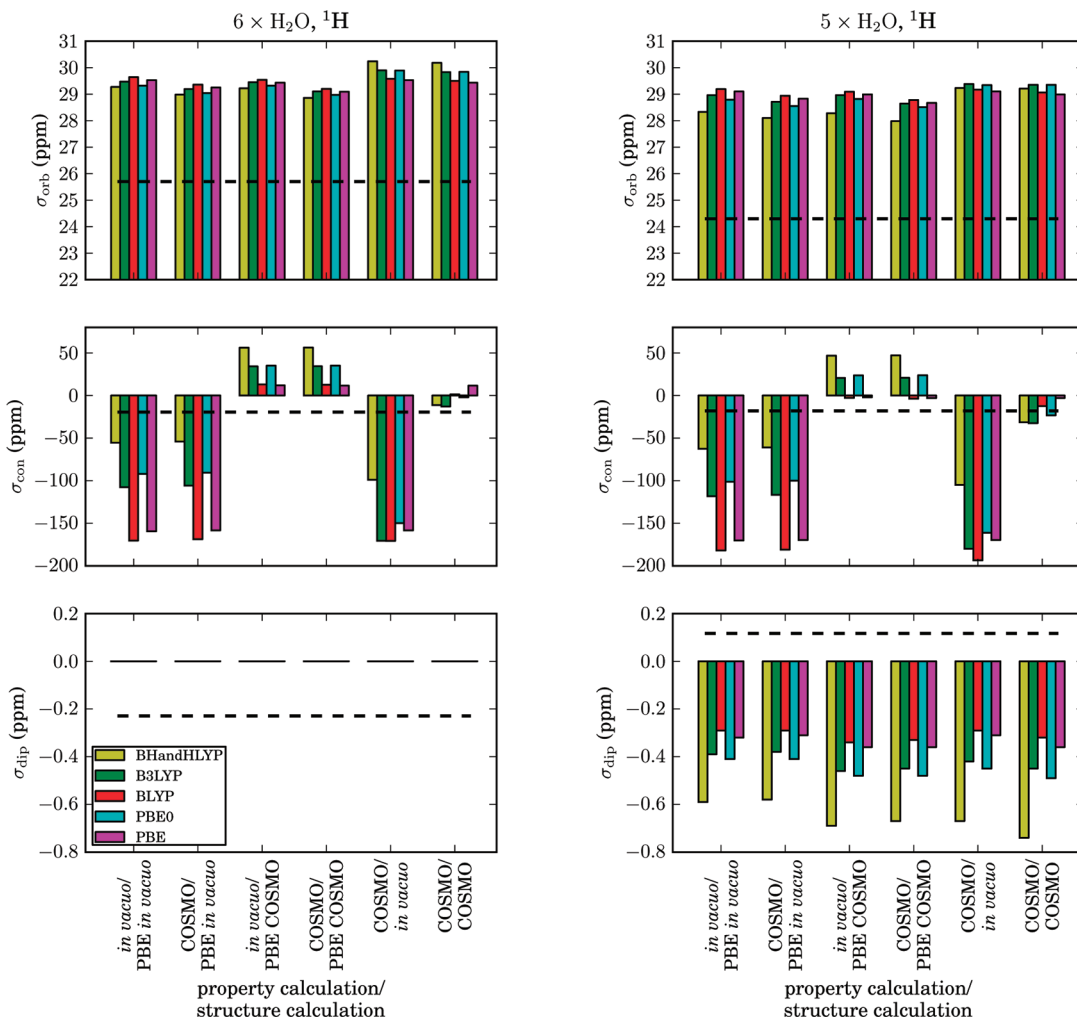


Figure 8. Impact of the choice of the DFT exchange-correlation functional on the average orbital (orb), contact (con), and dipole (dip) parts of the ^1H isotropic shielding constant (ppm) in $\text{Ni}(\text{H}_2\text{O})_n^{2+}$ ($n = 5, 6$). Here, σ_{con} consists of the sum of isotropic values of σ_{con} , $\sigma_{\text{con},2}$, and $\sigma_{\text{con},3}$ terms; σ_{dip} is calculated in an analogous way by summing isotropic values of σ_{dip} , $\sigma_{\text{dip},2}$, $\sigma_{\text{dip},3}$, and σ_{pc} (Table S1, Supporting Information).

ref 25 for higher than doublet spin multiplicities play an unimportant role in the present triplet system.

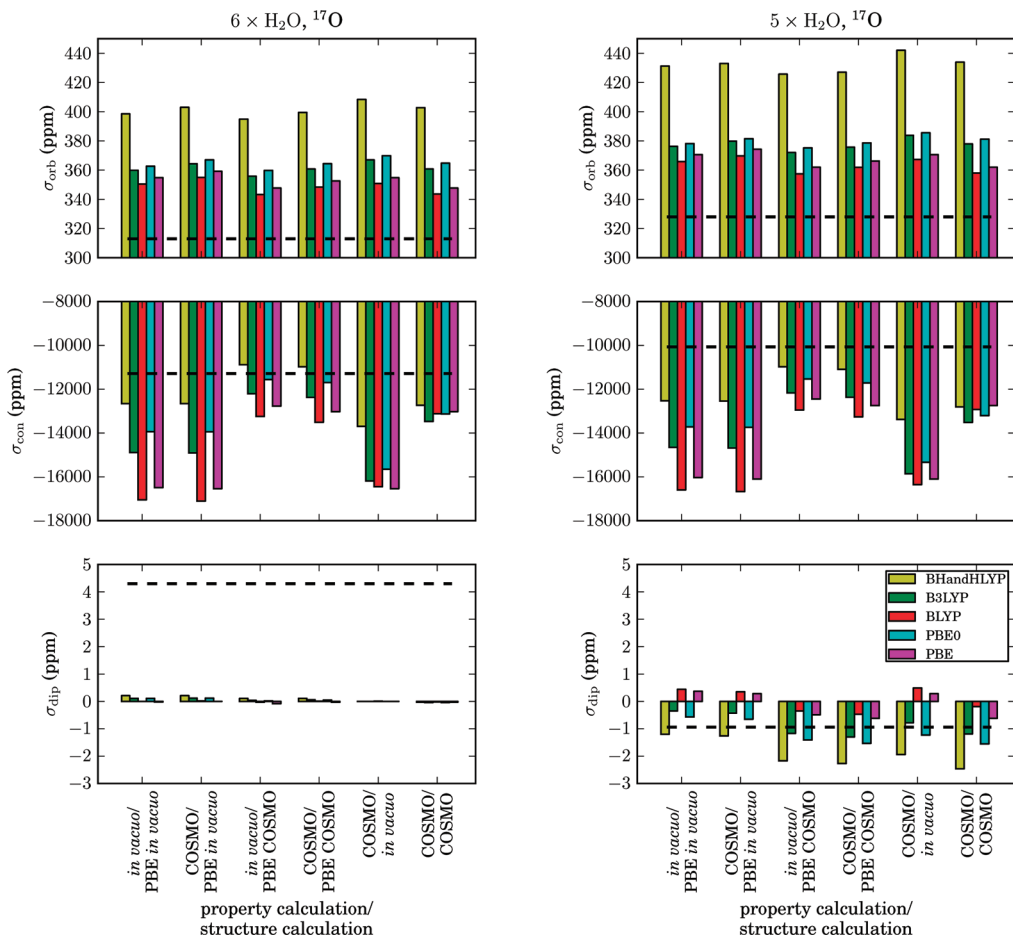
The smallest range of the total σ is again observed for the structures obtained with the COSMO model and using the same functional by which the property calculations were performed. Due to the ambiguity of the $A_{\text{con}}(^1\text{H})$, the final $\sigma(^1\text{H})$ in FSS remains somewhat vaguely determined, in the range of 15–39 ppm. The relative range pertaining to ^{17}O is smaller, and the final results are between –11200 and –10500 ppm.

Reducing the FSS of the Ni^{2+} ion from six to five water molecules, a decrease is observed for the orbital shielding of the ^1H nuclei (Figure 8, up-most panels), whereas an increase is seen for ^{17}O for all of the tested combinations of static structures and functionals, as well as for the averages from the FPMD trajectory (Figure 9, up-most panels). The sum of the isotropic contact contributions σ_{con} follows the behavior of A_{con} . Hence, there is only very little change at ^1H nuclei and decrease in magnitude for ^{17}O .

The sum of the isotropic dipolar contributions (σ_{dip} , $\sigma_{\text{dip},2}$, $\sigma_{\text{dip},3}$, and σ_{pc}) gives a negligible average for the highly symmetric 6-fold-coordinated structures because of the negligible differences in the ZFS energy levels. Nonzero values are obtained for

the 5-fold coordinated structures, which reflects the behavior of the ZFS tensor. Among these terms, the σ_{pc} term strongly dominates for ^1H in 5-fold situations. For the ^{17}O nucleus, the magnitudes of σ_{dip} and σ_{pc} are similar for the 6-fold coordinated structure, whereas the σ_{pc} term dominates in the 5-fold structure. Also, from the FPMD trajectory, small but nonvanishing average values of the isotropic dipolar shielding are obtained for both nuclei.

Nuclear Shielding in MD Snapshot Calculations. An analysis of the nuclear shielding terms obtained from the FPMD simulation is presented in Tables 3 and 4. The same orbital and contact terms are seen to give significant contributions in the dynamic solvation data as for the static structures. We again observe a dominant contact contribution to the isotropic pNMR shielding for both ^1H and ^{17}O nuclei, in both FSS and SSS. For both ^1H and ^{17}O in FSS, the second largest contribution is due to the $\text{con},3$ term originating from the SO correction to \mathbf{g} . The $\text{con},2$ term, which is related to the SO correction of A , also contributes significantly. It is noteworthy that the dynamic FSS contact shielding of –20 ppm differs clearly from the corresponding static models of FSS (Table S6, Supporting Information), where the use of the COSMO model consistently

Figure 9. As for Figure 8, but for ${}^{17}\text{O}$.Table 3. Total Isotropic ${}^1\text{H}$ and ${}^{17}\text{O}$ Nuclear Magnetic Resonance Shielding Constants, Error Margins, and Contributions from Different Physical Mechanisms for Atoms in the First and Second Solvation Shells of the Aqueous Solution of the Ni^{2+} Ion^a

symbol	term in σ_{et}^b	atom (shell)			
		${}^1\text{H}$ (FSS)	${}^1\text{H}$ (SSS)	${}^{17}\text{O}$ (FSS)	${}^{17}\text{O}$ (SSS)
σ_{orb}	$\sigma_{\text{et}}^{\text{orb}}$	25.7 ± 0.1	25.64 ± 0.07	313 ± 1.0	269.2 ± 0.7
σ_{con}	$g_e A_{\text{con}} \langle S_e S_t \rangle_0$	-20 ± 4	0.4 ± 0.1	-10870 ± 90	-86 ± 8
σ_{dip}	$g_e \Sigma_b A_{\text{br}}^{\text{dip}} \langle S_e S_b \rangle_0$	-0.18 ± 0.09	-0.04 ± 0.03	4 ± 1	-0.08 ± 0.02
$\sigma_{\text{con},2}$	$g_e A_{\text{PC}} \langle S_e S_t \rangle_0$	1.57 ± 0.01	0.0145 ± 0.0005	121.3 ± 0.2	-0.68 ± 0.02
$\sigma_{\text{dip},2}$	$g_e \Sigma_b A_{\text{br}}^{\text{dip},2} \langle S_e S_b \rangle_0$	0.002 ± 0.004	-0.002 ± 0.001	0.11 ± 0.04	-0.004 ± 0.001
$\sigma_{\text{con},3}$	$\Delta g_{\text{iso}} A_{\text{con}} \langle S_e S_t \rangle_0$	-1.0 ± 0.1	0.022 ± 0.003	-534 ± 4	-4.28 ± 0.3
$\sigma_{\text{dip},3}$	$\Delta g_{\text{iso}} \Sigma_b A_{\text{br}}^{\text{dip}} \langle S_e S_b \rangle_0$	-0.008 ± 0.003	-0.002 ± 0.001	0.19 ± 0.04	-0.004 ± 0.001
σ_{caniso}	$A_{\text{con}} \Sigma_a \Delta \tilde{g}_{ea} \langle S_a S_t \rangle_0$	-0.0002 ± 0.0003	0.0 ± 0.0	-0.06 ± 0.06	0.0 ± 0.0
σ_{pc}	$\Sigma_{ab} \Delta \tilde{g}_{ea} A_{\text{br}}^{\text{dip}} \langle S_a S_b \rangle_0$	-0.043 ± 0.005	0.0 ± 0.0	0.00 ± 0.03	-0.001 ± 0.002
σ_{tot}		6 ± 4	26.1 ± 0.1	-10960 ± 90	177 ± 8

^a The numbers are calculated from the 2000 snapshots (sampled over ca. 80 ps) of the first-principles molecular dynamics trajectory using the PBE functional with 127 water molecules and one Ni^{2+} ion. In this part of the trajectory, the Ni^{2+} ion is six-fold-coordinated. Paramagnetic shielding was obtained using a formal temperature of 350 K. ^b Referring to the tensor component combinations of g and A that give rise to the listed terms. See ref 25 and the brief account of theory in the Supporting Information. See Table 2 for comparison with available experimental results.

for both structures and properties leads to ca. +9 ppm at the PBE level. Similarly as for A_{con} , $\sigma_{\text{con}} = +9$ ppm coincides well with the experimental value (7.68 ppm). [This number was obtained by assuming that the measured value is contact shift referenced with respect to the orbital shielding of pure water (*vide infra*).]

Taking into account the pronounced dependence of $A_{\text{con}}({}^1\text{H})$ on the used ECF, this is probably fortuitous. A similar observation applies to the orbital shielding, where the static model produces a value some 4 ppm larger than the present FPMD result, 25.7 ppm. These differences indicate that dynamics need to be

Table 4. As for Table 3 but for the Five-Fold-Coordinated Part of the Trajectory^a

symbol	term in σ_{et}	atom (shell)			
		¹ H (FSS)	¹ H (SSS)	¹⁷ O (FSS)	¹⁷ O (SSS)
σ_{orb}	σ_{et}^{orb}	24.3 ± 0.9	25.0 ± 0.3	328 ± 6	265 ± 3
σ_{con}	$g_e A_{con} \langle S_e S_t \rangle_0$	-19 ± 3	0.66 ± 0.05	-9709 ± 130	-56 ± 4
σ_{dip}	$g_e \sum_b A_{bt}^{\text{dip}} \langle S_e S_b \rangle_0$	0.08 ± 0.05	-0.025 ± 0.007	-0.3 ± 0.9	-0.008 ± 0.008
$\sigma_{con,2}$	$g_e A_{pc} \langle S_e S_t \rangle_0$	2.01 ± 0.04	0.025 ± 0.004	165 ± 1	-0.72 ± 0.08
$\sigma_{dip,2}$	$g_e \sum_b A_{bt}^{\text{dip},2} \langle S_e S_b \rangle_0$	0.013 ± 0.006	0.0 ± 0.0	0.17 ± 0.06	0.0 ± 0.0
$\sigma_{con,3}$	$\Delta g_{iso} A_{con} \langle S_e S_t \rangle_0$	-1.1 ± 0.15	0.036 ± 0.003	-525 ± 7	-3.1 ± 0.2
$\sigma_{dip,3}$	$\Delta g_{iso} \sum_b A_{bt}^{\text{dip}} \langle S_e S_b \rangle_0$	0.004 ± 0.003	-0.0014 ± 0.0004	-0.01 ± 0.05	-0.0005 ± 0.0009
$\sigma_{c,aniso}$	$A_{con} \sum_a \Delta \tilde{g}_e A_{at}^{\text{dip}} \langle S_a S_t \rangle_0$	-0.0006 ± 0.0002	0.0 ± 0.0	-0.19 ± 0.09	0.0 ± 0.0
σ_{pc}	$\sum_{ab} \Delta \tilde{g}_{ea} A_{bt}^{\text{dip}} \langle S_a S_b \rangle_0$	0.02 ± 0.02	0.009 ± 0.004	-0.8 ± 0.5	-0.003 ± 0.006
σ_{tot}		6 ± 3	25.7 ± 0.3	-9733 ± 130	204 ± 4

^a 120 snapshots over ca. 3 ps were used.**Table 5.** Principal Values of the Total ¹H and ¹⁷O Shielding Tensors and the Contributions of the Various Physical Mechanisms for Nuclei in the First (FSS) and Second (SSS) Solvation Shells in the Aqueous Solution of the Ni²⁺ Ion^a

	¹ H (FSS)			¹⁷ O (FSS)		
	σ_{orb}	σ_{con}	σ_{dip}	σ_{tot}	σ_{tot}	
σ_{orb}	21.9 ± 0.7	32.1 ± 0.9	20.6 ± 0.6	230 ± 7	317 ± 10	365 ± 12
σ_{con}	-29 ± 5	-29 ± 5	-28 ± 5	-11200 ± 200	-11300 ± 200	-10200 ± 200
σ_{dip}	-462 ± 3	149.4 ± 1.4	312 ± 2	-4590 ± 50	2390 ± 40	2200 ± 50
$\sigma_{con,2}$	1.63 ± 0.03	1.59 ± 0.03	1.65 ± 0.03	128 ± 2	129 ± 2	116 ± 3
$\sigma_{dip,2}$	-24.0 ± 0.2	13.7 ± 0.2	10.29 ± 0.14	-171 ± 3	59 ± 6	112 ± 7
σ_{ac}	0.006 ± 0.008	-0.007 ± 0.007	0.001 ± 0.005	-0.07 ± 0.09	0.01 ± 0.08	0.06 ± 0.04
$\sigma_{con,3}$	-1.4 ± 0.3	-1.4 ± 0.2	-1.4 ± 0.3	-557 ± 8	-563 ± 8	-506 ± 10
$\sigma_{dip,3}$	-23.0 ± 0.2	7.45 ± 0.09	15.57 ± 0.14	-229 ± 3	119 ± 2	110 ± 3
$\sigma_{c,aniso}$	0.011 ± 0.013	-0.038 ± 0.014	0.03 ± 0.02	-1.1 ± 1.3	1 ± 2	-1 ± 2
σ_{pc}	-0.07 ± 0.02	0.024 ± 0.009	-0.09 ± 0.03	-0.4 ± 0.5	-0.1 ± 0.5	0.4 ± 0.4
σ_{tot}	-515 ± 6	174 ± 5	331 ± 6	-16400 ± 200	-8900 ± 200	-7800 ± 200

	¹ H (SSS)			¹⁷ O (SSS)		
	σ_{orb}	σ_{con}	σ_{dip}	σ_{tot}	σ_{tot}	
σ_{orb}	22.5 ± 0.8	18.8 ± 0.8	35.2 ± 1.3	254 ± 7	251 ± 7	276 ± 8
σ_{con}	0.62 ± 0.10	0.62 ± 0.10	0.68 ± 0.10	-82 ± 5	-81 ± 5	-78 ± 5
σ_{dip}	-99.3 ± 0.9	48.6 ± 0.5	50.7 ± 0.7	-146 ± 2	58.9 ± 1.3	87 ± 1
$\sigma_{con,2}$	0.016 ± 0.002	0.016 ± 0.002	0.017 ± 0.002	-0.70 ± 0.03	-0.69 ± 0.03	-0.69 ± 0.03
$\sigma_{dip,2}$	-5.16 ± 0.07	2.55 ± 0.04	2.61 ± 0.04	-4.06 ± 0.07	2.32 ± 0.05	1.73 ± 0.06
σ_{ac}	0.003 ± 0.002	-0.002 ± 0.002	-0.0002 ± 0.0007	0.000 ± 0.003	-0.004 ± 0.002	0.004 ± 0.002
$\sigma_{con,3}$	0.031 ± 0.005	0.031 ± 0.005	0.034 ± 0.005	-4.1 ± 0.3	-4.0 ± 0.2	-3.9 ± 0.2
$\sigma_{dip,3}$	-4.96 ± 0.06	2.43 ± 0.03	2.53 ± 0.04	-7.31 ± 0.14	2.94 ± 0.07	4.37 ± 0.09
$\sigma_{c,aniso}$	-0.0004 ± 0.0002	0.0000 ± 0.0002	0.0006 ± 0.0003	-0.024 ± 0.011	0.006 ± 0.011	0.011 ± 0.011
σ_{pc}	-0.003 ± 0.005	-0.011 ± 0.005	0.018 ± 0.008	-0.022 ± 0.008	-0.004 ± 0.007	-0.001 ± 0.007
σ_{tot}	-86.2 ± 1.4	73.0 ± 0.9	91.8 ± 1.1	10 ± 10	230 ± 9	287 ± 9

^a See also Tables 3 and 4. Since there is no unique principal axis frame of the shielding tensors, which would be preserved through the simulation time for a particular molecule, the averages are calculated from principal values sorted according to the magnitude of the instantaneous principal values of the total shielding in the order $\sigma_{11}^{\text{tot}} \leq \sigma_{22}^{\text{tot}} \leq \sigma_{33}^{\text{tot}}$.

accounted for in proton shielding in FSS; i.e., the static models are not capable of yielding quantitative results. In contrast, the ¹⁷O shielding shows a rather modest, systematic shift of ca. 1700 ppm (13%) for contact and 34 ppm (10%) for orbital shielding, for the 6-fold-coordinated Ni²⁺ ion. The ¹H nuclei are expectedly more sensitive to dynamical solvation effects than ¹⁷O.

Both ¹H and ¹⁷O shieldings undergo a dramatic change from FSS to SSS. Whereas the FSS shieldings are governed by the

paramagnetic hyperfine effects, their magnitude decreases in SSS to a level comparable to the orbital shielding. The second shell deviates, however, still significantly from diamagnetic bulk water in the large σ_{con} contributions of 0.4 and -86 ppm for ¹H and ¹⁷O, respectively.

There is a significant difference between the isotropic dipolar shielding in static calculations of Ni(H₂O)₆²⁺ (Figures 8 and 9) and the average of snapshot calculations. The absolute value of

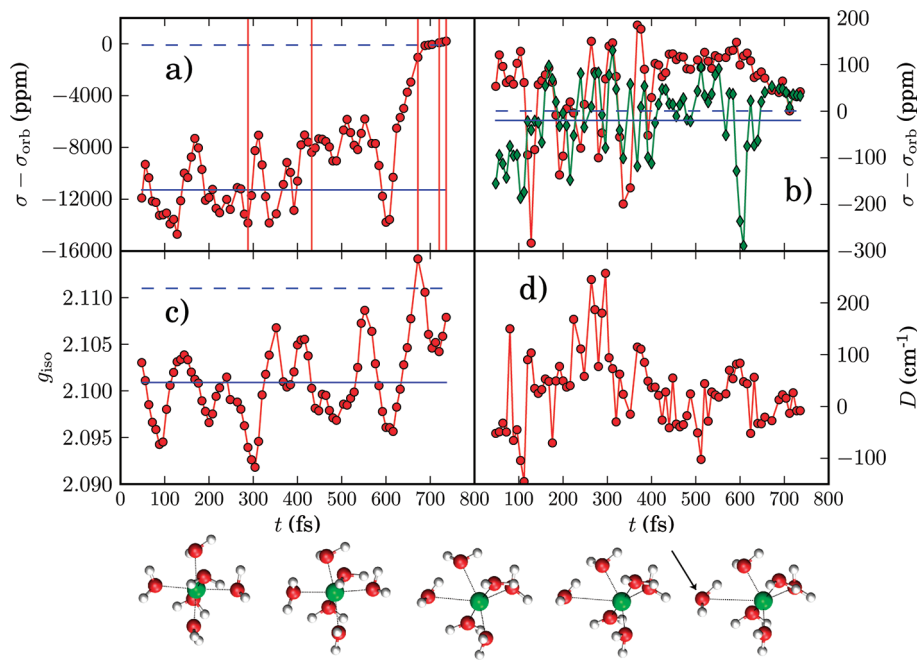


Figure 10. Calculated hyperfine part of the (a) ^{17}O and (b) ^1H isotropic paramagnetic shielding constants (in ppm) together with (c) g value and (d) D parameter of zero-field splitting along the final stages of a first-principles molecular dynamics trajectory of an aqueous solution of the Ni^{2+} ion. The PBE functional was used for a system with 127 water molecules. In particular, the end of the trajectory segment includes the event of the water molecules leaving the first solvation shell. The shielding constants in panels a and b correspond to this molecule (the ^1H shielding constants are plotted for both water protons separately). The five vertical bars in panel a indicate the times appropriate for the depicted structures. The solid blue horizontal lines indicate the first solvation shell averages of the shielding constants, whereas the dashed horizontal lines show values corresponding to the second shell. The arrow at the last depicted structure identifies the departing water molecule. In panel c, the isotropic g value is illustrated together with the averages in 6-fold (solid line) and 5-fold (dashed line) coordinated parts of the trajectory. Panel d visualizes the D parameter of the zero-field splitting tensor.

σ_{dip} is much larger in the latter although still very small compared to the total shielding. This difference is caused by the fluctuation in ZFS in the instantaneous snapshot calculations.

To facilitate comparison with published experimental chemical shift data, we calculated the diamagnetic reference shielding of the H_2O molecule *in vacuo* using the equilibrium structure obtained at the same level and using the same program and settings as were used for the FPMD simulation. The resulting geometrical parameters are $r_{\text{OH}} = 0.978 \text{ \AA}$ and $\angle_{\text{HOH}} = 102.45^\circ$. The shielding calculation using this geometry at the PBE/IGLO-II level yields $\sigma_{\text{O}} = 324.8$ and $\sigma_{\text{H}} = 31.59$ ppm. Furthermore, we used the calculated B3LYP values for the gas-to-liquid transition⁶ $\delta_{\text{g} \rightarrow \text{l}}(^1\text{H}) = -5.27$ ppm and $\delta_{\text{g} \rightarrow \text{l}}(^{17}\text{O}) = -41.2$ ppm to obtain a gross estimate of the liquid-state shielding constants of the bulk diamagnetic water, $\sigma_{\text{O}}^{\text{ref}}(1) = 283.6$ ppm, $\sigma_{\text{H}}^{\text{ref}}(1) = 26.32$ ppm. These reference values were used to obtain the shielding value from the published chemical shift data for the aqueous solution of Ni^{2+} ($\sigma_{\text{exp}} = \sigma_{\text{ref}} - \delta_{\text{exp}}$). To obtain the experimental shielding values at 350 K, at which the presented simulated shielding values were calculated, the experimental shieldings were extrapolated using the $1/T$ dependence of the paramagnetic shielding. The simulated shielding constants in FSS can then be directly compared with the experimental shielding constants σ_{exp} obtained from the chemical shift of the water molecules. The results listed in Table 2 indicate that in the presence of the Ni^{2+} ion the calculated ^{17}O shielding constant agrees with the experimental data of Neely and Connick³⁵ and to a somewhat lesser extent also with those of Fiat and Chmelnick,³⁸ whereas the simulated ^1H shielding constant does not reproduce the experimental data of Granot.³¹

Table 5 lists the simulated contributions of the various physical mechanisms of pNMR shielding to the principal values σ_{ii} ($i = 1, 2, 3$) of the shielding tensor. There are important contributions to the principal values beyond those that are significant for the isotropic values. Despite their negligible isotropic averages, the dipole terms assume the same role here as played by the contact terms in σ_{iso} . The σ_{dip} term contributes to the diagonal values almost comparably to the largest (σ_{con}) term for ^{17}O in FSS. Also, the terms originating in the SO corrections to \mathbf{A} and \mathbf{g} , $\sigma_{\text{dip},2}$ and $\sigma_{\text{dip},3}$, respectively, are important for ^{17}O (FSS). For ^{17}O (SSS), the σ_{ii}^{dip} even exceeds σ_{con} in magnitude. The ^1H nuclei in SSS obtain shielding eigenvalues of σ_{dip} larger by 1 or 2 orders of magnitude than the corresponding contact terms. In the present isotropic solution, these large anisotropic dipolar terms with negligible isotropic averages only contribute to NMR relaxation, and not to the structure of static NMR spectra. The water molecules in SSS still experience significantly anisotropic shielding interactions originating from the paramagnetic ion. We note that despite the fact that σ_{con} is formally anisotropic in the novel nuclear shielding theory,²⁸ in practice its eigenvalues are equal within the present statistical error margins. The σ_{ac} term, which is formally not contributing to the isotropic σ , is negligible also for the eigenvalues. [At this point, it is worth it to point out the effect of the averaging described in Table 5. When the principal axis system (PAS) of the individual shielding contribution is not identical to the PAS of the total shielding, the reported projected average values tend to be biased toward their respective isotropic values. After analyzing this issue, we conclude that the majority of the shielding contributions have closely similar PASs on average. Among paramagnetic contributions, there are two exceptions,

$\sigma_{c,\text{aniso}}$ and σ_{pc} . Both are related to the g-shift tensor anisotropy ($\Delta\tilde{\mathbf{g}}$). Those yield in their own PAS average principal values roughly 1 order of magnitude larger compared to those numbers present in Table 5. Since even these numbers are small compared to the principal numbers of the total shielding, we do not report a more detailed analysis here. The PAS of the “diamagnetic” orbital shielding is expectedly also different from the total shielding, and the effect is different in FSS and SSS, according to the relative magnitude of the orbital and paramagnetic shielding in these shells.] The ^1H orbital shielding eigenvalues reveal that despite similar isotropic averages in FSS, SSS, and diamagnetic water, the tensors in FSS and SSS differ significantly.

Dipolar Part of the Hyperfine Interaction. Due to the fundamental importance of A_{dip} in paramagnetic relaxation studies, we present here a few notes about its calculation in the simple point-dipole approximation (PDA) as opposed to the present QM method. Correlation graphs between the QM (PBE) calculation and PDA are plotted in Figure S2, Supporting Information. It can be seen that for ^1H , PDA becomes a very good approximation for the smallest values of A_{33}^{dip} ($\lesssim 1.3$ MHz) in the most distant regions of the SSS ($\gtrsim 5$ Å). On the other hand, the PDA for ^{17}O cannot be considered realistic. [We can anticipate that the quantum-mechanically obtained spin density at the ^{17}O nucleus is qualitatively correct from the agreement between the calculated and experimental contact contributions.] A similar conclusion can be obtained from Table S10, Supporting Information, where the angle between the main principal axis of A_{dip} for ^1H and ^{17}O and corresponding to the Ni–H or Ni–O axes is evaluated. In all of these cases, the two axes are on average close to being parallel. In SSS, however, this applies only for ^1H and the distribution of the angle is sufficiently narrow so that the geometry-based PDA may be useful. It is noteworthy that the O–H bond direction has no apparent significance for the main principal axis of $A_{\text{dip}}(^1\text{H})$.

The evolution along the MD trajectory of the largest principal value A_{33}^{dip} is plotted in Figure S3, Supporting Information. For each case, only one atom was selected. The changes at the end of the traces correspond to the transition from the 6- to the 5-fold-coordinated complex. In the case of ^1H SSS, the evolution of A_{33}^{dip} could be visually related to the evolution of the distance from the Ni^{2+} ion.

Magnetic Properties during the Exchange Event. The hyperfine shielding for the molecules departing from FSS as well as the evolution of the g value and the D parameter of ZFS are followed along the last part of the FPMD trajectory. Figure 10 shows the magnetic parameters at selected snapshots during the departure of the water molecule from FSS. It is seen that the shielding values approach the averages of SSS. In particular, the plot reflects the oscillations of the isotropic part of the hyperfine shielding. The corresponding fluctuations in the full shielding tensor are responsible for Curie-type pNMR relaxation. Likewise, Figure 10c illustrates the step taking place in the g value from the 6-fold to the 5-fold-coordinated situation.

■ CONCLUSIONS

Using first-principles computations, we have investigated the magnetic properties of the aqueous solution of Ni^{2+} . Both static quantum-chemical calculations of the hexa- and penta-aqua complexes $\text{Ni}(\text{H}_2\text{O})_n^{2+}$ ($n = 5, 6$), as well as first-principles molecular dynamics simulation of the aqueous solution, were performed to obtain structures for the calculation of magnetic

properties. These include all factors affecting the paramagnetic nuclear shielding tensor. The first principles trajectory used for snapshot calculations is the longest of its kind so far, for systems and properties of the present type.

We tested several combinations of methods for the calculation of ESR properties (hyperfine couplings, zero-field splitting, and g tensor), which were subsequently used for the calculation of paramagnetic NMR shielding according to the recent general theory. The spin density distribution of the solvated Ni^{2+} decays rapidly to zero over the first and second solvation shells. We observe that the dominant Fermi contact hyperfine interaction of the hydrogen atoms in the first solvation shell is very sensitive to structure, in particular the tilt angle of the water molecules. Depending on the method used for the static structures, results in the range covering 1 order of magnitude, depending on the tilt angle, are observed. It therefore proved to be beneficial to combine methods for structure calculation and calculation of properties such that both share the same equilibrium geometry, to reduce the range of results and to obtain a well-defined ^1H isotropic hyperfine data. To the contrary, the dipolar ^1H as well as both the contact and dipolar ^{17}O results are less sensitive to the methods used. In particular, the static calculations indicated little influence of the implicit solvation model at the property evaluation step, and the primary influence arises indirectly via the structure.

We compared properties calculated using the 5- and 6-fold-coordinated model structures as well as 5- and 6-fold-coordinated parts of the FPMD trajectory. Upon the transition from 6- to 5-fold-coordination, the eigenvalues of $A_{\text{dip}}(^1\text{H})$ experience a significant increase, whereas the change in $A_{\text{con}}(^1\text{H})$ is very small. The $A_{\text{dip}}(^{17}\text{O})$ eigenvalues are slightly decreased upon entering the 5-fold-coordinated structures, whereas the $A_{\text{con}}(^{17}\text{O})$ values decrease more significantly. The same behavior is followed by the corresponding shielding constants. The significant change of the isotropic ^{17}O shielding constant between the 6- and 5-fold-coordinated Ni^{2+} may be of importance from the experimental point of view. For example, high-pressure NMR determination of the parameters of water exchange in the aqueous Ni^{2+} complex assume σ_{iso} (as well as the underlying A_{iso} and g_{iso}) to be invariant for the different coordination cases. For A_{dip} , we also show that the point-like approximation becomes a good approximation for ^1H in the distant parts of the second solvation shell, at distances around 5 Å and further.

We have followed the g and ZFS tensors along the MD trajectory. Both parameters are very sensitive to the change of geometry and feature short correlation times. A notable feature at the water exchange event is the increase of the perpendicular components of the g tensor upon the transition to a five-coordinated Ni^{2+} ion. The trajectory averages of the g value are slightly above the values calculated for the optimized static 5- and 6-fold coordinated structures. The magnitude of the D parameter decreases significantly upon the transition to the 5-fold coordination. The same behavior is not seen for the static structure, where all 6-fold coordinated models are highly symmetric and show therefore very small zero-field splitting.

Both ^1H and ^{17}O isotropic shielding constants undergo a large change from the first to the second solvation shell. Whereas the FSS shieldings are dominated by the paramagnetic hyperfine effects, in SSS the orbital shielding is already the larger contribution. The situation is different for the shielding anisotropy, as seen from the principal values of the shielding tensors. Here, the dipolar contribution still is much larger than the orbital shielding

for ^1H in SSS. For ^{17}O , the principal values of σ_{dip} (and σ_{con}) are nearly of the same magnitude as σ_{orb} . Several new isotropic shielding contributions (as compared to the case of doublet³⁹) predicted for a higher-than-doublet system²⁵ proved to be very small for the current triplet system.

■ ASSOCIATED CONTENT

S Supporting Information. An extensive methods section, a brief summary of the theory of pNMR shielding, tables with numerical data, and additional figures. This material is available free of charge via the Internet at <http://pubs.acs.org>.

■ AUTHOR INFORMATION

Corresponding Author

*E-mail: jiri.mares@oulu.fi.

■ ACKNOWLEDGMENT

The authors thank Dr. Perttu Lantto and Dr. Matti Hanni (Oulu) for helpful discussions. The research leading to these results has received funding from the European Union Seventh Framework Programme (FP7/2007-2013) under grant agreement no. 254552. (J.M.) Further support was received from Swiss National Funds—project PBZHP2-125353 (J.M.), University of Helsinki Research Funds, and the University of Oulu. The authors belong to the Finnish Center of Excellence in Computational Molecular Science (CMS). Computational resources due to CSC (Espoo, Finland) were used.

■ REFERENCES

- (1) Hermansson, K.; Knuts, S.; Lindgren, J. *J. Chem. Phys.* **1991**, *95*, 7486.
- (2) Eggenberger, R.; Gerber, S.; Huber, H.; Searles, D.; Welker, M. *J. Chem. Phys.* **1992**, *97*, 5898.
- (3) Malkin, V. G.; Malkina, O. L.; Steinebrunner, G.; Huber, H. *Chem.—Eur. J.* **1996**, *2*, 452.
- (4) Bühl, M.; Parrinello, M. *Chem.—Eur. J.* **2001**, *7*, 4487.
- (5) Bühl, M.; Mauschick, F. T. *Phys. Chem. Chem. Phys.* **2002**, *4*, 5508.
- (6) Pennanen, T. S.; Vaara, J.; Lantto, P.; Sillanpää, A.; Laasonen, K.; Jokisaari, J. *J. Am. Chem. Soc.* **2004**, *126*, 11093.
- (7) Ramalho, T. C.; Bühl, M. *Magn. Reson. Chem.* **2005**, *43*, 139.
- (8) Vaara, J. *Phys. Chem. Chem. Phys.* **2007**, *9*, 5399.
- (9) Asher, J. R.; Kaupp, M. *Theor. Chem. Acc.* **2008**, *119*, 477.
- (10) Schmidt, J.; Hutter, J.; Spiess, H.; Sebastiani, D. *ChemPhysChem* **2008**, *9*, 2313.
- (11) Odelius, M.; Ribbing, C.; Kowalewski, J. *J. Chem. Phys.* **1995**, *103*, 1800.
- (12) Yazyev, O. V.; Helm, L. *J. Chem. Phys.* **2006**, *125*, 54503.
- (13) Yazyev, O. V.; Helm, L. *J. Chem. Phys.* **2007**, *127*, 84506.
- (14) Lindgren, M.; Laaksonen, A.; Westlund, P. *Phys. Chem. Chem. Phys.* **2009**, *11*, 10368.
- (15) Kowalewski, J.; Larsson, T.; Westlund, P. O. *J. Magn. Reson.* **1987**, *74*, 56.
- (16) Odelius, M.; Ribbing, C.; Kowalewski, J. *J. Chem. Phys.* **1996**, *104*, 3181.
- (17) Kowalewski, J.; Egorov, A.; Kruk, D.; Laaksonen, A.; Aski, S. N.; Parigi, G.; Westlund, P. *J. Magn. Reson.* **2008**, *195*, 103.
- (18) Kruk, D.; Kowalewski, J. *J. Chem. Phys.* **2002**, *116*, 4079.
- (19) Kruk, D.; Kowalewski, J.; Westlund, P. *J. Chem. Phys.* **2004**, *121*, 2215.
- (20) Kruk, D.; Kowalewski, J. *J. Chem. Phys.* **2009**, *130*, 174104.
- (21) Yazyev, O. V.; Helm, L. *Eur. J. Inorg. Chem.* **2008**, *2008*, 201.
- (22) Clore, G. M.; Iwahara, J. *Chem. Rev.* **2009**, *109*, 4108.
- (23) Mareš, J.; Liimatainen, H.; Laasonen, K.; Vaara, J. *J. Chem. Theory Comput.* **2011**, in press; doi: 10.1021/ct200320z.
- (24) Kowalewski, J.; Mäler, L. *Nuclear Spin Relaxation in Liquids: Theory, Experiments, and Applications*, 1st ed.; Taylor & Francis: United Kingdom, 2006; p 440.
- (25) Pennanen, T. O.; Vaara, J. *Phys. Rev. Lett.* **2008**, *100*, 133002.
- (26) Munzarová, M.; Kaupp, M. *J. Phys. Chem. A* **1999**, *103*, 9966.
- (27) Neese, F. ORCA; University of Bonn: Bonn, Germany, 2009.
- (28) Frisch, M. J. et al. Gaussian 03, revision C.02.; Gaussian Inc.: Wallingford, CT, 2009.
- (29) VandeVondele, J.; Krack, M.; Mohamed, F.; Parrinello, M.; Chassaing, T.; Hutter, J. *Comput. Phys. Commun.* **2005**, *167*, 103.
- (30) Helgaker, T.; Jaszunski, M. *J. Chem. Theory Comput.* **2007**, *3*, 86.
- (31) Granot, J. *J. Chem. Phys.* **1974**, *61*, 3043.
- (32) Gauss, J.; Källay, M.; Neese, F. *J. Phys. Chem. A* **2009**, *113*, 11541.
- (33) Griffiths, J. H. E.; Owen, J. *Proc. R. Soc. London, Ser. A* **1952**, *213*, 459.
- (34) Friedman, H. L.; Holz, M.; Hertz, H. G. *J. Chem. Phys.* **1979**, *70*, 3369.
- (35) Neely, J. W.; Connick, R. E. *J. Am. Chem. Soc.* **1972**, *94*, 3419.
- (36) Blumberg, W. E. In *Magnetic Resonance in Biological Systems*, 1st ed.; Ehrenberg, A., Malmström, B., Eds.; Pergamon Press: Oxford, U.K., 1967; p 110.
- (37) Neese, F. In *Calculation of NMR and EPR Parameters: Theory and Applications*, 1st ed.; Kaupp, M., Bühl, M., Malkin, V. G., Eds.; Wiley-VCH: New York, 2004; p 541.
- (38) Fiat, D.; Chmelnick, A. M. *J. Am. Chem. Soc.* **1971**, *93*, 2875.
- (39) Pennanen, T. O.; Vaara, J. *J. Chem. Phys.* **2005**, *123*, 174102.